BIOCHEMISTRY
including biophysical chemistry & molecular biology

Article

pubs.acs.org/biochemistry

Characterization and Modeling of the Oligomeric State and Ligand Binding Behavior of Purified Translocator Protein 18 kDa from *Rhodobacter sphaeroides*

Fei Li,[†] Yan Xia,[‡] Jens Meiler,[‡] and Shelagh Ferguson-Miller*[,†]

[†]Department of Biochemistry and Molecular Biology, Michigan State University, East Lansing, Michigan 48824, United States

[‡]Department of Chemistry, Center for Structural Biology, 465 21st Avenue South, BIOSCI/MRBIII, Vanderbilt University, Nashville, Tennessee 37232, United States

Supporting Information

ABSTRACT: Translocator Protein 18 kDa (TSPO), previously known as the peripheral-type benzodiazepine receptor (PBR), is a mitochondrial outer membrane protein that has been identified as a key player in cholesterol and porphyrin transport, apoptotic signaling, and cancer development, as well as neurological inflammation and disease. Despite a number of TSPO ligands whose effects have been studied with respect to these varied biological activities, the nature of their interactions with TSPO and the molecular mechanism of their effects remain controversial, in part because of the lack of an atomic-resolution structure. We expressed and purified the homologue of mammalian TSPO from *Rhodobacter sphaeroides* (*Rs*TSPO), as well as a mutant form in a proposed drug binding loop, *Rs*TSPOW38C. We characterized their binding behaviors with endogenous ligands and a series of compounds that affect apoptosis by using a sensitive tryptophan fluorescence quenching assay. Our results show that *Rs*TSPO behaves as a dimer in the purified state and binds with low micromolar affinity to many of these ligands, including retinoic acid, curcumin, and a known Bcl-2 inhibitor, gossypol, suggesting a possible direct role for TSPO in their regulation of apoptosis. A computational model of the *Rs*TSPO dimer is constructed using EM-Fold, Rosetta, and a cryo-electron microscopy density map. Binding behaviors of known ligands are discussed in the context of the model with respect to regions that may be involved in binding.

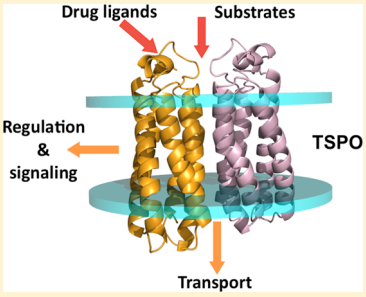

Translocator Protein 18 kDa (TSPO) was originally discovered as a secondary binding site for the widely prescribed antianxiety drugs, benzodiazepines, in the mitochondria of rat kidney.[1] For this reason, it became known as the peripheral-type benzodiazepine receptor (PBR). In 2006, it was renamed Translocator Protein 18 kDa (TSPO)[2] to better represent the emerging understanding of a family of highly conserved integral membrane proteins (Figure 1) found from Archaea to plants and humans, with a broad spectrum of functions, including steroid and porphyrin transport and regulation of apoptosis, inflammation, metastatic cancer, and cardiovascular diseases.[3,4]

In mammalian cells, TSPO is primarily located in the outer mitochondrial membrane and concentrated at the outer−inner membrane contact sites.[5] It is expressed in all organs examined so far and at particularly high levels in steroid hormone-producing tissues, such as adrenal glands and kidney. Knockout of TSPO is developmentally lethal in the mouse.[6] The major function of TSPO has been proposed to be transporting small molecules, including cholesterol and heme biosynthesis intermediates, into or out of mitochondria to be further metabolized.[7−10] In addition, TSPO has been found to be strongly expressed in areas of brain injury and inflammation,[11] and in aggressive cancers,[12,13] as well as brains of Alzheimer and Huntington disease patients.[14] In these situations, TSPO has been proposed to be involved in the regulation of the mitochondrial permeability transition pore (MPTP),[15,16] thus exerting its effects on cellular homeostasis (see reviews in *Current Molecular Medicine*[17,18]). TSPO ligands, including benzodiazepines and more specific compounds represented by the diagnostic ligand PK11195, have been shown to attenuate cancer cell proliferation,[13] to have neuroprotective effects,[19] and to inhibit the MPTP.[20] The interaction of TSPO with ligands continues to be a strong research focus aimed at the development of drugs targeting TSPO for imaging and treatment of diverse disease states.

Mitochondria play important roles in the normal function of cells and also in regulating cell death through apoptosis and/or necrosis.[21,22] The initiation of apoptosis is usually preceded by a loss of the mitochondrial membrane potential ($\Delta\Psi_m$), which is proposed to be regulated by the MPTP,[23] a multiprotein complex whose structural components are still not established. Together with other proteins, TSPO has been implicated as a regulator of the MPTP, having been isolated originally in a complex with the voltage-dependent anion channel (VDAC) and the adenine nucleotide translocator (ANT).[24] Both VDAC and ANT are candidate components of the MPTP,[15,25] but

Received: April 5, 2013
Revised: July 11, 2013
Published: August 16, 2013

   dx.doi.org/10.1021/bi400431t | *Biochemistry* 2013, 52, 5884−5899

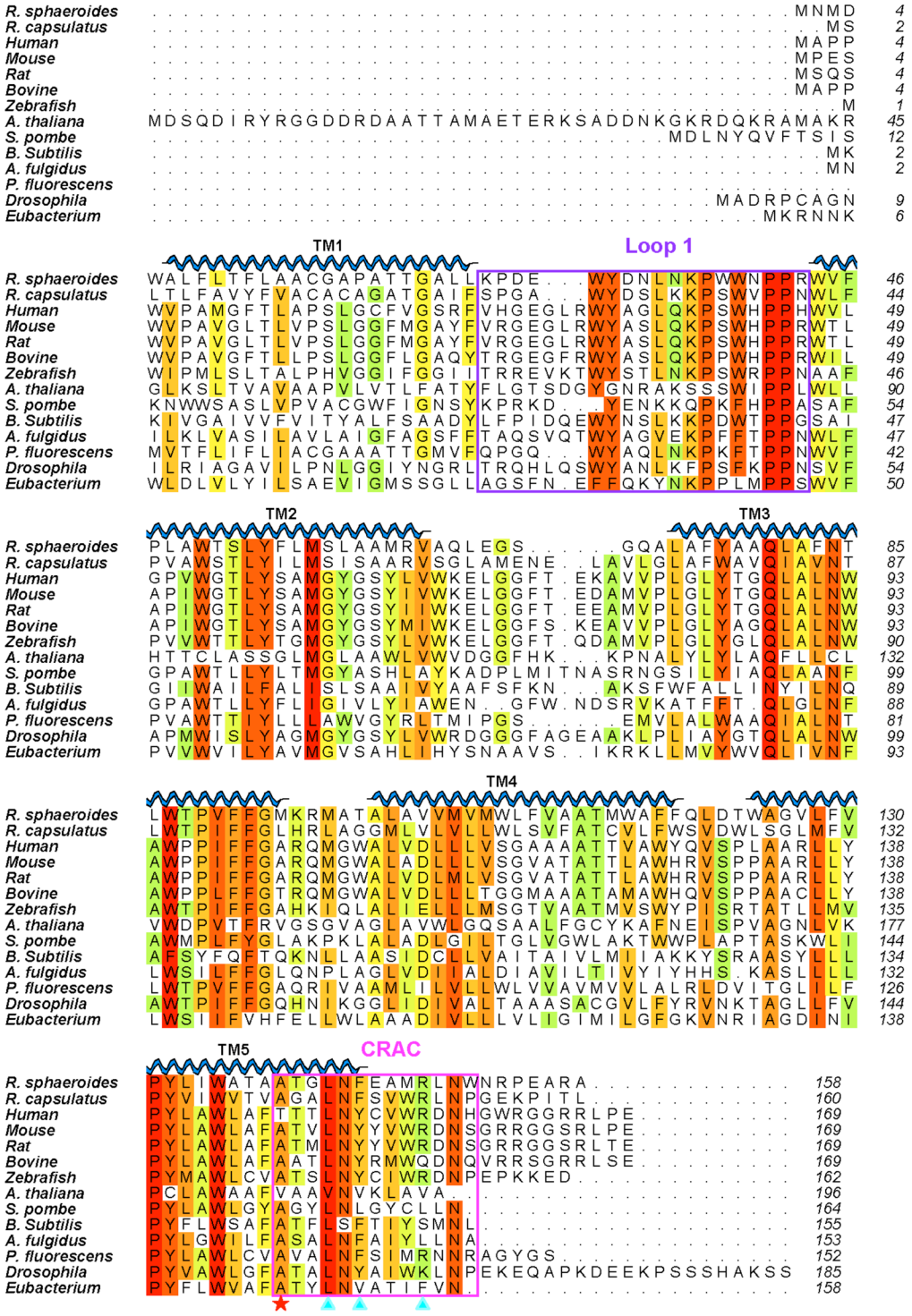

Figure 1. Sequence alignment of TSPO proteins. Shown in the alignment are TSPO proteins from *Rhodobacter sphaeroides* 2.4.1 (AAF24291), *Rhodobacter capsulatus* (Z11165), human (CAB55884), mouse (NP_033905), rat (NP_036647), bovine (DAA29060), zebrafish (NP_001006032), *Arabidopsis thaliana* (AAL16286), *Schizosaccharomyces pombe* (CAA22182.2), *Bacillus subtilis* (YP_004204918.1), *Archaeoglobus fulgidus* (NP_070304.1), *Pseudomonas fluorescens* (YP_348542.1), *Drosophila melanogaster* (AAF51482), and *Eubacterium siraeum* DSM 15702 (EDS01113.1). Conserved amino acids are colored from deep red to yellow. The secondary structure is predicted on the basis of the sequence of *Rs*TSPO by the server Toppred.[81] Transmembrane helices are labeled on top of the sequences. The cholesterol recognition/interaction amino acid consensus (CRAC) is highlighted in a magenta rectangular box with the three critical amino acids labeled with cyan triangles. The proposed drug/porphyrin binding loop (loop 1) is highlighted in a purple rectangular box. The red star denotes the position of the human A147T polymorphism. The alignment was made using the CLUSTALW server, and the image was created in Aline.[82]

other possibilities remain.[26] Various TSPO ligands have been shown to regulate apoptosis;[27] however, it is currently still unclear how MPTP or apoptosis is regulated by TSPO.

In the purple non-sulfur bacteria that are proposed to be ancestors of mitochondria,[28] TSPO was discovered in the carotenoid gene cluster as CrtK,[29] first in *Rhodobacter*

dx.doi.org/10.1021/bi400431t | *Biochemistry* 2013, 52, 5884−5899

capsulatus[29,30] and subsequently in *Rhodobacter sphaeroides* (*Rs*TSPO).[31] Initially designated as the tryptophan-rich sensory protein (TspO), the bacterial protein was recognized as being homologous to the mitochondrial PBR.[30,31] In *Rhodobacter*, it is located in the outer membrane and involved in regulating photosynthetic gene expression in response to oxygen and light conditions.[32,33] Similar to its mammalian ortholog, *Rs*TSPO is proposed to be involved in the transport of small molecules such as porphyrin intermediates of the heme and chlorophyll biosynthesis−degradation pathways.[33,34] *Rs*TSPO shares considerable sequence homology with human TSPO (*Hs*TSPO) (Figure 1), and rat TSPO has been shown to substitute for *Rs*TSPO in *R. sphaeroides*, suggesting a functional link.[32] Along with an overall significant level of sequence identity (30%), *Rs*TSPO shares noteworthy sequence similarity with *Hs*TSPO in the first extramembrane loop (loop 1) that is proposed to participate in porphyrin[34] and drug binding,[35] as well as in the cholesterol binding site located at the cholesterol recognition/interaction amino acid consensus (CRAC) sequence at the C-terminus, including the end of transmembrane helix V.[36]

Although *R. sphaeroides* does not make cholesterol, it does produce a related class of steroid-like molecules, hopanoids,[37] which may account for why the proposed critical residues for cholesterol binding are well-conserved between mammalian TSPO and *Rs*TSPO. However, the sequences before and after the CRAC region vary. A recent paper reported that the human A147T single polymorphism immediately preceding the CRAC sequence in helix V resulted in reduction in affinity for a PK11195 analogue used for PET imaging of 2 orders of magnitude.[38] This finding highlights the adjacent variable region (residues 144−146 in the human sequence) that could play a role in differences in ligand binding between *Rhodobacter* and human TSPO. In addition, loop 1, implicated in drug and porphyrin binding by mutations in both *Rhodobacter*[34] and mammalian[35] TSPO, is highly variable in the initial one-third, while the rest is conserved. Differences in this region may also play a role in the significantly higher affinity of PK11195 reported for human[39] and for rat TSPO expressed in *R. sphaeroides* compared to the endogenous *Rs*TSPO.[32] In addition, the W38C mutation in this loop 1 region was observed to influence the dimerization and stability of *Rs*TSPO, suggesting a complex role in protein structure.[34] With respect to cholesterol binding, information about the binding behavior of *Rs*TSPO is still not available, and the possibility of direct or allosteric competition among PK11195, cholesterol, and porphyrin has been suggested[40] but not established.

Discrepancies and controversies remain in the literature regarding the binding of TSPO ligands and the physiological significance of their interactions.[35,41,42] For instance, TSPO ligands have been reported to have pro-apoptotic effects in cancer cells[43] but to be anti-apoptotic in cardiac tissue after ischemia and reperfusion injury.[20,44,45] A major difficulty comes from the interpretation of binding data measured in complex systems such as total membranes or whole cells from different tissues where other proteins may affect the interaction. To clarify some of these issues, we have expressed and purified to homogeneity wild-type *Rs*TSPO and the reported dimer-stabilizing mutant W38C.[34] We describe studies of their oligomerization state as well as their binding to ligands, including cholesterol, porphyrin, the diagnostic drug PK11195, and a series of compounds with reported apoptosis-influencing properties. Using a sensitive tryptophan fluorescence quenching assay, our results show that these ligands have direct interactions with *Rs*TSPO at micromolar affinity. We provide an atomic-level model of the *Rs*TSPO dimer, based on a 10 Å resolution cryo-electron microscopy (cryo-EM) density map[46] and using EM-Fold,[47] and discuss the relationship between ligand interactions in the context of the dimer model. Some novel ligands characterized in this study provide candidates for the optimization of crystallization of TSPO.

MATERIALS AND METHODS

Materials. Chemicals were purchased from Sigma-Aldrich (St. Louis, MO). Dodecyl maltoside (DDM), decyl maltoside (DM), and *n*-dodecylphosphocholine (Fos-Choline-12) (Anagrade) were purchased from Anatrace (Maumee, OH). The *Rs*TSPO expression plasmid was a gift from S. Kaplan from the University of Texas (Austin, TX), and codon-optimized *Hs*TSPO was synthesized by DNA 2.0. Pfu Turbo polymerase was purchased from Agilent technologies (Santa Clara, CA). Restriction enzymes and T4 ligase were purchased from New England Biolabs (Ipswich, MA).

Cloning. The coding sequence of *Rs*TSPO was subcloned into the pUC12 vector for mutagenesis. The W38C mutant of *Rs*TSPO was made by QuikChange mutagenesis (Stratagene). Fusion protein constructs were made by the splicing-by-overlapping-extension method.[48] Primers used in the polymerase chain reaction are listed in Table T1 of the Supporting Information. Constructs were confirmed by sequencing and ligated into the pRK415 expression vector with KpnI and HindIII restriction sites or the pJ411 (DNA 2.0) expression vector with NdeI and EcoRI restriction sites. The human TSPO gene was codon optimized for *Escherichia coli* expression and purchased from DNA 2.0 in the pJ411 vector. Expression vectors containing the desired TSPO coding sequence were confirmed by sequencing and introduced into *E. coli* expression strain BL21 λDE3.

Protein Expression and Purification. The transformed bacteria were cultured at 30 °C in 100 mL of LB medium containing the appropriate antibiotics overnight. Fifteen milliliters of the overnight culture was then transferred into 1 L of autoinduction medium (ZYM-5025)[49] containing glycerol, glucose, lactose, and the appropriate antibiotics. Cultures were grown at 30 °C for *Rs*TSPO, *Rs*TSPOW38C, and fusion proteins, and the temperature was decreased to 12 °C for *Hs*TSPO to reduce the level of inclusion bodies and GroEL. Cells were harvested when the OD_{600} exceeded 4.0. Harvested cells were resuspended in lysis buffer [50 mM KH_2PO_4 (pH 6.5) and 1 mM EDTA] supplemented with Roche protease inhibitor cocktail and lysed via two passes at 20000 psi through a French press homogenizer. Broken cells were centrifuged at 200*g* for 5 min, 10000*g* for 30 min, and 150000*g* for 90 min at 4 °C to isolate the membranes. Isolated membranes were resuspended with buffer A [50 mM Tris-HCl (pH 8), 150 mM NaCl, and 10% glycerol], quick frozen with liquid nitrogen, and stored at −70 °C before being purified.

Membranes were thawed on ice, resuspended to a total protein concentration of 10 mg/mL in buffer A, solubilized via addition of 1% DDM, 1 mM PMSF, and Roche protease inhibitor cocktail (no EDTA), and stirred at 4 °C for 1 h. Solubilized membranes were centrifuged at 150000*g* for 30 min to remove the unsolubilized fraction. The supernatant was loaded on a 10 mL Ni-NTA (Qiagen) gravity column pre-equilibrated with buffer A. After being extensively washed with buffer A supplemented with 0.2% DM and 50 mM imidazole, fractions containing the desired protein were eluted using

buffer A supplemented with 0.2% DM and 300 mM imidazole over 2 column volumes. Fractions containing the desired protein were pooled, concentrated with a 50 kDa cutoff Amicon Filter (Millipore), washed once with buffer A supplemented with 0.2% DM, and diluted to 10 mL. Trypsin was added at a rate of 0.2 mg/mg of *Rs*TSPO10ht, and the protein solution was incubated at 4 °C overnight. Trypsin-treated *Rs*TSPO10ht was concentrated to 250 μL with a 30 kDa cutoff Amicon filter and loaded onto a Superose 12 300/10 gel filtration column (GE Life Sciences) pre-equilibrated with buffer B [50 mM Tris-HCl (pH 8.0), 150 mM NaCl, 0.2% DM, and 2 mM β-mercaptoethanol (βME)] and run at 0.3 mL/min. The homogeneous peak fractions of *Rs*TSPO were pooled, and the concentration of the protein was determined by the UV absorbance at 280 nm. The purity of the protein was estimated via sodium dodecyl sulfate−polyacrylamide gel electrophoresis (SDS−PAGE) stained with Coomassie blue. The average yield of wild-type *Rs*TSPO was 5 mg/L of culture. *Rs*TSPO was also solublized and purified in Fos-Choline-12 (2 and 0.2%) using the same buffer conditions but without the SEC step. This version of the protein was used for comparative binding experiments (Figure 9).

Codon-optimized *Hs*TSPO was expressed at good levels in *E. coli* and was purified in the same way as *Rs*TSPO. However, the *E. coli* chaperone protein GroEL was found to be copurified with *Hs*TSPO as a persistent contaminant. As shown in Figure S1 of the Supporting Information, a reasonably pure *Hs*TSPO monomer with a trace of dimer was present in the sample, but with a significant amount of GroEL copurified (Figure S1 of the Supporting Information). The fortuitous absence of tryptophan in GroEL, combined with the unusually high tryptophan content of TSPO (13 of 169 amino acids), made it possible to conduct some ligand binding studies with the human protein based on fluorescence quenching, but not to characterize its oligomeric state.

Light Scattering Measurements of the Oligomeric State of Purified *Rs*TSPO. A static light scattering method combined with UV absorption and refractive index measurement was used to investigate the oligomeric state of purified *Rs*TSPO.[50] Four microliters of a 30 mg/mL purified *Rs*TSPO sample was loaded on a Superdex 200 300/10 column coupled with the triple detector array (Malvern) and run in buffer B at a rate of 0.3 mL/min at 4 °C. Purified ovalbumin and pure DM were run in the same buffer under the same conditions. Data were analyzed in OmniSEC to calculate the molecular mass of the protein−detergent complex and the fraction of protein by comparing the light scattering, which represents the size of the protein−detergent complex, and the amount of proteins in the complex as measured by UV_{280} (ε = 71960 M^{-1} cm^{-1}).

Tryptophan Fluorescence Quenching Binding Assay. A tryptophan fluorescence quenching assay was used to study the binding properties of TSPO by utilizing the intrinsic tryptophan fluorescence.[46] For *Rs*TSPO and *Rs*TSPOW38C, 2.5 μM purified protein was titrated with increasing amounts of ligand in the desired concentration range at room temperature. Each titration point was monitored by a spectral scan from 290 to 400 nm (excitation at 285 nm) on a PTI QuantaMaster spectrofluorimeter. Control experiments were performed to evaluate the absorption and emission of ligands as well as buffers and solvents. Because of the slight shift of the tryptophan fluorescence peak during the experiment caused by differential quenching of buried tryptophans versus solvent-exposed tryptophans, the area under each emission spectrum was integrated to account for all tryptophans and a percentage quenching ratio for each concentration was calculated. The binding curve was obtained by plotting the percentage quenching (%Quen) versus the total ligand concentration ($[L_t]$) in Origin. Equation 1 was derived on the basis of a single binding site per monomer assumption, taking into consideration ligand depletion. $[L_t]$ is the total ligand concentration plotted on the binding curves. The calculation of K_d is corrected by eq 1 for ligand depletion, which occurs at low ligand concentrations because of the relatively high protein:ligand ratio.

$$\%\text{Quen} = \text{Offs} + F_{max}\{[f[P_t] + [L_t] + K_d - \sqrt{(f[P_t] + [L_t] + K_d)^2 - 4f[P_t][L_t]}\,]/(2f[P_t])\} \quad (1)$$

$$F_{max} = \frac{F_i - F_f}{F_i} \quad (2)$$

where %Quen represents the calculated percentage quenching at each concentration, F_{max} is the maximal amplitude of fluorescence quenching, which equals the difference between the initial and final fluorescence signals divided by the initial fluorescence, $[L_t]$ is the total ligand concentration, $[P_t]$ is the total concentration of purified *Rs*TSPO protein (fixed at 2.5 μM in the experiment and during the fitting procedure), and K_d is the apparent dissociation constant. Offs (offset) allows a fit unconstrained to go through zero, while f is a parameter to account for the effective fraction of protein involved in binding. Offs and f help to optimize the fitting by accounting for binding modes involving different numbers of sites. For partially purified *Hs*TSPO with a total protein concentration at 2.5 μM, the binding curve was obtained the same way as for *Rs*TSPO, but the apparent dissociation constant (K_{app}) was estimated as the concentration of the half-maximal quenching, because it is assumed that nonspecific binding to contaminating GroEL may give a K_{app} that is larger than the actual value. These *Hs*TSPO experiments were conducted with a mutant, C153E, that removed the possible complication of the extra cysteine in the human protein and that showed no difference in terms of expression, purification, or reported function. All ligands are dissolved in DMSO as a stock solution and diluted with DMSO or buffer for measurement except for cholesterol and PpIX, which were dissolved in pure ethanol and 0.15 M NaCl, respectively. Control quenching curves with solvent alone were determined. One representative binding curve is shown in each figure, while the K_d is reported as the average of three replicate measurements fitted with eq 1.

Modeling of the *Rs*TSPO Dimer. The experimental EM density map from the EM database (EMDB entry 1698) was processed in Chimera[51] to match published helix placement in a *Rs*TSPO dimer density. Final models were generated using a modified protocol from Lindert et al.[47] Twenty thousand decoys were generated using a simultaneously combined BCL::EM-Fold and the membrane protein protocol in BCL::MP-fold.[52] Briefly, the transmembrane helices were first assembled into the density rods as a monomer. The models were evaluated by their agreement with the density map as well as a knowledge-based potential. The models were then clustered combining all models with the same arrangement of transmembrane helices (topology). The 150 top-scoring topologies were then symmetrized and subjected to another round of EM-fold refinement against the density map. The full-

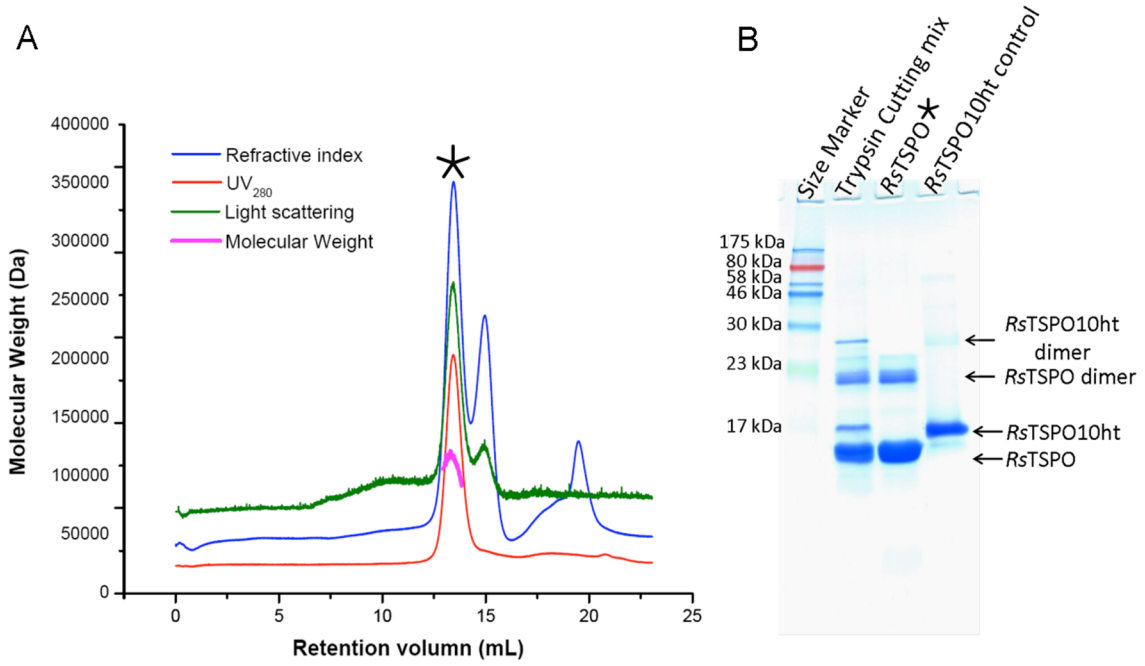

Figure 2. Purification and determination of the molecular mass of *Rs*TSPO. (A) One representative trace of purified *Rs*TSPO on the triple detector array (Malvern). The peak of *Rs*TSPO is labeled with a star, and the molecular mass was calculated as described and expressed on the *Y* axis. (B) SDS–PAGE for the purification of *Rs*TSPO. The lane of SEC-purified *Rs*TSPO is labeled with a star corresponding to the light scattering profile. The trypsin cutting mix represents the sample before SEC, while a purified *Rs*TSPO10ht sample was used as the control.

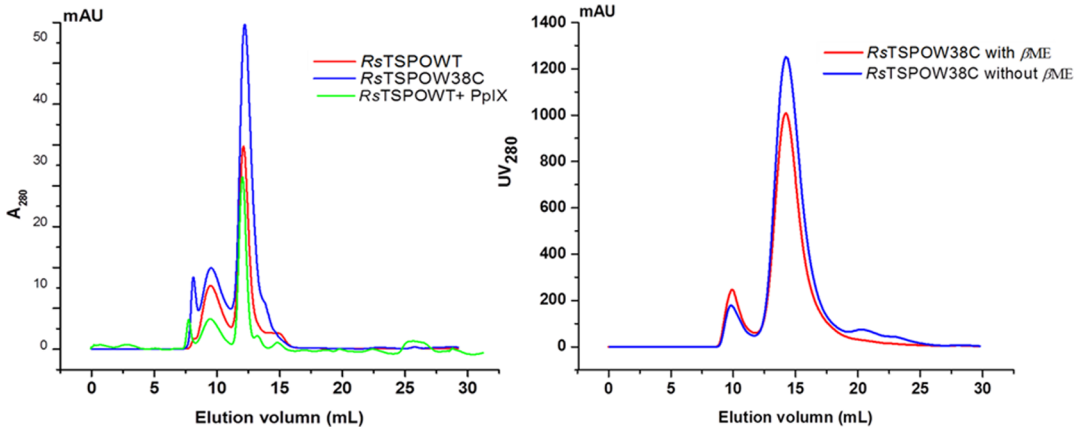

Figure 3. Investigation of the oligomeric state of purified *Rs*TSPO by SEC. (A) SEC profile of wild-type *Rs*TSPO, *Rs*TSPOW38C, and wild-type *Rs*TSPO in the presence of 350 μM PpIX on a prepacked Superose 12 300/10 column. (B) SEC profile of *Rs*TSPOW38C in the presence and absence of βME on a homemade Superose 12 column.

atom models were generated using Rosetta;[53,54] of the 150 refined topological folds from the previous step, 75 top-scoring folds were used to generate 2000 all-atom models per fold. Then, within each topology, the models were clustered with respect to loop conformation. For the 20 top-scoring loop conformations from each of the 75 topologies, three rounds of iterative loop modeling, side chain repacking, and relaxation were conducted using the density map as a restraint in Rosetta.[47,54] Twenty-five models were created in each iteration, and the top-scoring models were moved forward to the next iteration. The final models were ranked by the Rosetta full-atom energy score.[53−55] All figures were generated in Pymol version 1.3. The simulation did not test topologies that include domain swaps.

RESULTS

***Rs*TSPO Forms a Dimer *in Vitro*.** *Rs*TSPO was successfully purified to homogeneity by nickel affinity followed by size exclusion chromatography (SEC) (Figures 2 and 3A). The molecular mass of purified *Rs*TSPO with a 10-histidine tag was determined to be 19371.76 ± 1.77 Da (17910.26 Da for untagged *Rs*TSPO) by mass spectrometry, correlating well with the calculated molecular mass from the amino acid sequence (19347.58 Da). The SEC running profile in 0.2% DM showed a peak that suggested a dimer form based on elution profile and molecular mass standards. To obtain a more accurate estimate of the size of *Rs*TSPO, we characterized the purified *Rs*TSPO in solution by using a combination of light scattering, UV, and refractive index measurements. A representative run of the UV_{280}, refractive index, and light scattering measurements is shown in Figure 2A, and a representative SDS–PAGE gel is

dx.doi.org/10.1021/bi400431t | *Biochemistry* 2013, 52, 5884−5899

shown in Figure 2B. The molecular mass of the *Rs*TSPO–detergent complex was determined to be ~100 kDa from the scattering peak, with a protein fraction of ~36% from comparison of scattering and 280 nm absorption; therefore, the molecular mass of the *Rs*TSPO protein in the complex was calculated to be 37 kDa, indicating a dimer of *Rs*TSPO (given a monomer of 18 kDa) within the protein–detergent complex (Table 1). Purified ovalbumin and pure DM were also characterized under the same conditions. Ovalbumin showed a calculated molecular mass of ~44 kDa as a monomer, and DM showed a micelle size of ~37 kDa; both agreed very well with literature values and are consistent with the equivalent of approximately two micelles of DM in the dimer–detergent complex.

Table 1. Molecular Mass Calculation from Static Light Scattering Measurements

sample	$M_{wcomplex}$ [a]	$f_{protein}$ [b]	$M_{wprotein}$ [c]	monomer M_{wcal} [d]	$N_{monomer}$ [e]
*Rs*TSPO					
first	98430	0.347	34155	17976	1.9
second	104029	0.365	37971	17976	2.1
third	97328	0.372	36206	17976	2.0
fourth	111620	0.362	40406	17976	2.2
average	102852	0.3615	37181	17976	2.1
ovalbumin standard	42757	0.982	41987	44287	0.95
DM standard	37243	0	NA	NA	NA

[a]Molecular mass of the protein–detergent complex. [b]Fraction of protein in the protein–detergent complex. [c]Molecular mass of the protein without detergent. [d]Molecular mass calculated from sequence. [e]Number of protein monomers in the protein–detergent complex.

The question of whether ligands influence the oligomeric state was investigated by incubating the *Rs*TSPO with the ligand PpIX prior to SEC. The SEC trace in the presence of PpIX showed the same size as that of the protein without ligand (Figure 3A). Since Yeliseev and Kaplan reported the W38C mutant stabilizes a dimer form in *R. sphaeroides*,[34] a further question was whether a disulfide bond was involved in dimer formation, either through the W38C mutant or through the naturally existing cysteine, C15, in the first transmembrane helix. There was in fact no apparent change in the amount or stability of the dimer form in the W38C mutant and no effect of addition of βME, as evidenced by the lack of a difference in the elution profile from SEC (Figure 3A,B). Therefore, a disulfide bond is unlikely to be important in dimer formation.

These observations and the lack of a detectable monomer form in SEC suggest that the dimer organization of *Rs*TSPO in the DM micelle is a very strong association, but through interactions other than disulfide bonds and independent of ligand binding. The persistence of a small fraction of dimer even in the SDS gels run under strongly denaturing conditions also attests to the stability of the dimer.

We further explored the structure of the dimer *in vivo* by expressing in *E. coli* a dimer created by a gene fusion of two monomers. Three fusion proteins of *Rs*TSPO and *Hs*TSPO were constructed by making a direct connection between the C- and N-termini, resulting in a dimer with an antiparallel configuration (Figure S2A of the Supporting Information) as suggested to occur in the case of EmrE,[56] a possible alternative to the parallel configuration supported by the cryo-EM and our modeling studies of TSPO (see below). *E. coli* cells carrying the gene fusion constructs were characterized by Western blotting with antibodies against the histidine tag at the C-terminus of the fusion proteins. Our results show that the full-length fusion proteins with *Rs*TSPO at the C-terminus and human or *Rhodobacter* at the N-terminus (*Hs*–*Rs*TSPO and *Rs*–*Rs*TSPO) were expressed (Figure S2B of the Supporting Information) and inserted into the membrane without formation of a significant amount of inclusion bodies, implying a folded structure. In contrast, the dimer with the *Hs*TSPO portion at the C-terminus (*Rs*–*Hs*TSPO) was not detected, suggesting that this version of the fusion protein may not be correctly folded or inserted into the membrane.

Although these results tell us little about the significance or existence of an antiparallel dimer of TSPO, the observation that expression and insertion of the dimer depends on whether the *Rs* or *Hs* protein is at the C-terminus does suggest that membrane insertion of TSPO involves a C-terminal mechanism that may require additional machinery in the case of the mammalian protein, consistent with other evidence.[57−59]

Overall, our studies are consistent with the dimer being the major structural unit of *Rs*TSPO as also implied by the cryo-EM studies of the purified *Rs*TSPO and our modeling analysis, which indicate a parallel dimer.[46] The possibility of an

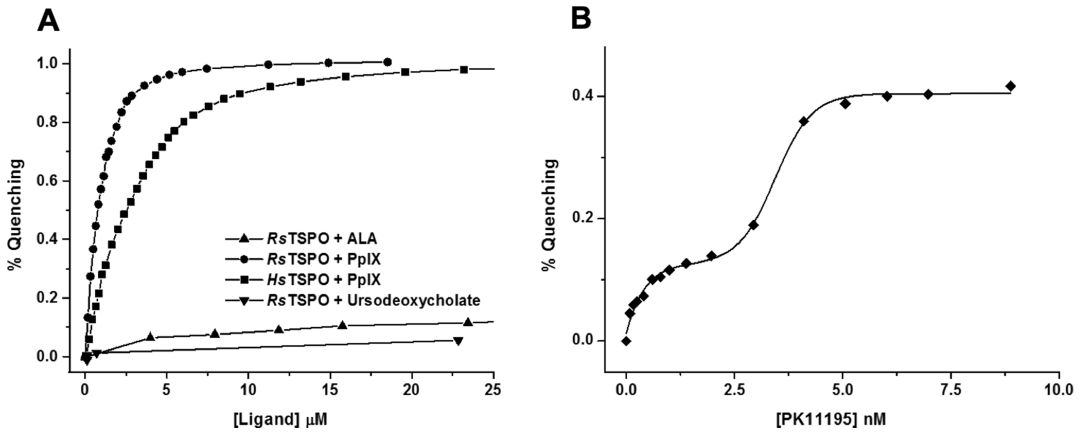

Figure 4. Binding of PpIX, ALA, and ursodeoxycholate to *Rs*TSPO and binding of PK11195 and PpIX to *Hs*TSPO. (A) Binding of PpIX, ALA, and ursodeoxycholate to purified *Rs*TSPO and PpIX to partially purified *Hs*TSPO measured with the tryptophan fluorescence quenching assay. (B) Binding of PK11195 to partially purified *Hs*TSPO.

dx.doi.org/10.1021/bi400431t | *Biochemistry* 2013, 52, 5884−5899

antiparallel dimer and other homo- or hetero-oligomeric forms in the native membrane remains to be explored.

Tryptophan Fluorescence Quenching Assay as a Sensitive Measure of K_d. We tested the validity of the tryptophan fluorescence quenching assay by measuring the binding of the known ligand, protoporphyrin IX (PpIX), to purified *Rs*TSPO (Figure 4A). We determined a K_d for PpIX of 0.3 μM, lower than that reported by Korkhov et al.[46] (8.6 μM), possibly indicating the sensitivity of binding behavior to a variety of assay conditions (see Discussion). The nonligand porphyrin precursor δ-aminolevulinic acid (ALA) and the solvent DMSO were also measured and showed only a small quenching of the tryptophan fluorescence compared to that of PpIX, as did the steroid ursodeoxycholate (see below). A similar low micromolar K_{app} for PpIX (2.4 μM) was also obtained with *Hs*TSPO (Figure 4A), a result within the range of previous reports of PpIX binding affinity for mammalian TSPO.[40,60] [The presence of the contaminating protein GroEL, which has no tryptophan and does not contribute to the fluorescence (see Materials and Methods), may, however, give a somewhat higher binding constant for *Hs*TSPO because of ligand depletion.]

We also tested the sensitivity of the assay by measuring the binding of *Hs*TSPO to the diagnostic ligand PK11195 with expected binding affinity in the nanomolar range. Our measurements show two K_{app} values of ~0.2 and 5 nM for PK11195 (Figure 4B), which agree with previous reports,[35] and two different nanomolar binding affinities for PK11195 in both mouse liver[8] and a human Leydig cell line.[61] The results demonstrate the ability of the assay to characterize high-affinity binding.

Effect of Detergent Conditions on the Binding Assay. It was also important to find detergent conditions that maintained a stable protein and were compatible with the assay. The nanomolar binding affinity of PK11195 for *Hs*TSPO (Figure 4B) was measured in 0.2% DM. However, a previous report suggested that binding of PK11195 with mouse TSPO in the detergent SDS resulted in a complete loss of affinity, emphasizing the importance of detergent conditions.[39] We tested the binding of PK11195 with *Rs*TSPO in two different concentrations of DM, as well as in the common detergent used in NMR, Fos-Choline-12 (Figure 5). In 0.1% DM, the binding affinity of purified *Rs*TSPO for PK11195 (10 μM) was slightly increased compared to that of 0.2% DM (7 μM), while Fos-Choline-12 lowered the affinity to ~120 μM. Therefore, for standard assay conditions for a comparison of ligands, 0.2% DM was selected to keep purified *Rs*TSPO stable while exhibiting good affinity for PK11195 [0.1% DM is just below the critical micelle concentration (CMC) of DM and has a tendency to allow protein precipitation over time].

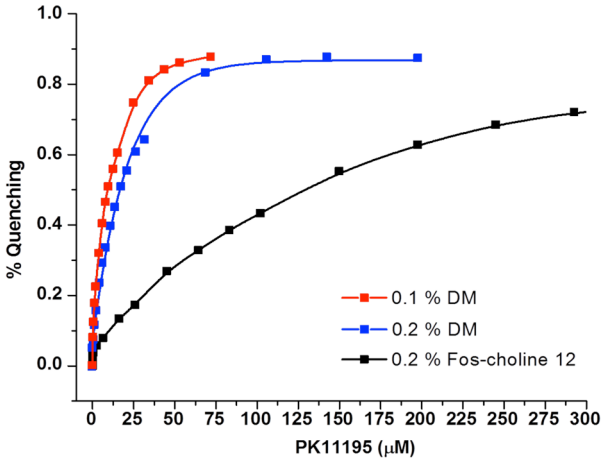

Figure 5. Binding curves of PK11195 with *Rs*TSPO under different detergent conditions as described in Materials and Methods.

***Rs*TSPO Binds PK11195 and Cholesterol with Micromolar Affinity.** In a pioneering study in 1997,[32] Yeliseev and colleagues reported that rat TSPO overexpressed in *R. sphaeroides* 2.4.1 displayed an affinity for PK11195 ranging from 4 to 12 nM, while wild-type *Rs*TSPO showed no binding affinity above background. However, in our studies with purified *Rs*TSPO, the binding affinity of PK11195 was found to be 10 ± 1 μM, suggesting a binding site in *Rs*TSPO with lower but significant affinity compared to those of the mammalian proteins (Figure 6 and Table 2). In addition, the

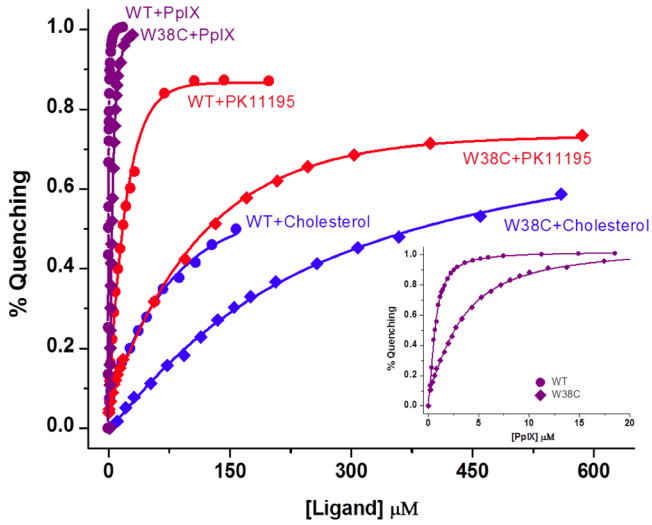

Figure 6. Binding of PpIX, PK11195, and cholesterol to purified *Rs*TSPO (WT) and *Rs*TSPOW38C (W38C). All binding curves were obtained and plotted as described in Materials and Methods. The inset shows a close-up of the 0–20 μM region to better show the binding curve of the PpIX.

*Rs*TSPO form containing a W38C mutation located in the middle of loop 1 where both PpIX and PK11195 are proposed to bind[34,35] decreased the binding affinity of PK11195 by 3-fold. These results indicate that loop 1 contributes to PK11195 binding. Binding of PpIX to *Rs*TSPO was also influenced by the W38C mutation (Figure 6 and Table 2), showing a 6-fold decrease in affinity (from 2 to 0.3 μM), consistent with both binding sites involving W38C in the conserved region of loop 1. Although it is suggested PK11195 and PpIX bind in the same general area (loop 1) in both *Rs*TSPO and *Hs*TSPO, it should be noted that loop 1 is predicted to be flexible and shorter in *Rs*TSPO than in *Hs*TSPO, and the corresponding residue of W38 in *Hs*TSPO is S41. These differences would be expected to impact the affinity and specificity of ligand binding.

Because cholesterol does not naturally occur in *Rhodobacter*, no data have been reported for its binding to *Rs*TSPO. However, *Rhodobacter* is one of the closest ancestors of mitochondria[28] and in fact has structural and functional analogues of cholesterol, hopanoids,[37] in the membrane where *Rs*TSPO is located. In addition, the TSPO sequence alignment (Figure 1) shows a remarkably high degree of

dx.doi.org/10.1021/bi400431t | *Biochemistry* 2013, 52, 5884–5899

Table 2. Structures and K_d Values of Ligands to Wild-Type *Rs*TSPO and Its W38C Mutant[2]

ligands	Structure	*Kd* to *Rs*TSPO (μM)	*Kd* to *Rs*TSPOW38C (μM)
Bilirubin	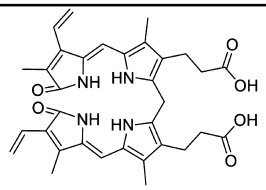	4.7 ± 0.2	5.5 ± 0.3
Cholesterol	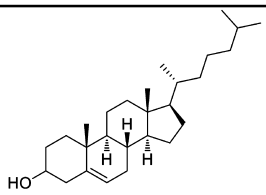	*Kapp* = 80 [1]	*Kapp* = 200 [1]
Curcumin	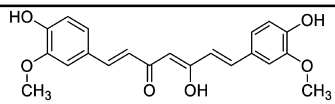	1.4 ± 0.1	2.6 ± 0.1
Gossypol	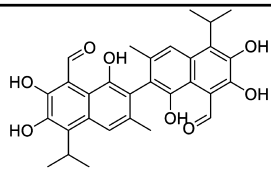	6.0 ± 0.2	3.9 ± 0.3
PK11195	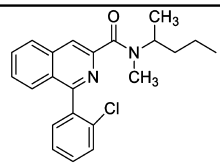	10 ± 1	34 ± 2
Protoporphyrin IX (PpIX)	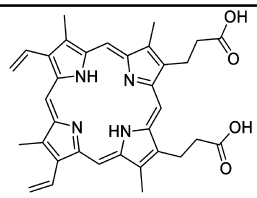	0.31 ± 0.01	2.0 ± 0.07
Retinoic acid	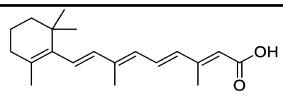	0.50 ± 0.02	1.6 ± 0.1

[1] K_{app} was estimated from half-maximal quenching. [2] K_d was obtained from fitting three independent titrations with eq 1, and the standard error is reported.

similarity at the proposed cholesterol binding site [CRAC, -L/V-$(X)_{1-5}$-Y-$(X)_{1-5}$-R/K-][36,62] across many species. In particular, two of the three proposed critical residues in the CRAC sequence (Leu and Arg) are identical between *Rs*TSPO and *Hs*TSPO while the other is a conservative substitution of phenylalanine for tyrosine. Therefore, we expected that *Rs*TSPO might also bind cholesterol. Because of the low solubility of cholesterol in aqueous solution, we were unable to determine an accurate K_d, but we estimate from the binding curve K_{app} values of ∼80 μM for wild-type *Rs*TSPO and ∼200 μM for the W38C mutant (Figure 6), significantly lower than the affinity reported for mammalian TSPO,[27] possibly because of the variable region immediately preceding the CRAC sequence in helix V (residues 144−147), including the site of a human polymorphism.[38,63] In contrast, the steroid derivative ursodeoxycholate showed no detectable affinity for *Rs*TSPO (Figure 4A), suggesting that the binding of cholesterol, albeit weak, is not just due to nonspecific interactions.

Competition Binding Assay of PpIX, PK11195, and Cholesterol. Loop 1 in the N-terminal region has been proposed to be where drugs and porphyrin bind,[27,64] while the cholesterol CRAC site is located in the C-terminal region of TSPO.[36] However, the small size of TSPO and the fact that it may function as a dimer or higher-order oligomer introduce the possibility that these two sites are very close to each other and interacting. Nevertheless, in the case of PpIX and PK11195, we observe some difference in spectroscopic properties in the binding assay. The tryptophan fluorescence of *Rs*- and *Hs*TSPO

dx.doi.org/10.1021/bi400431t | *Biochemistry* 2013, 52, 5884−5899

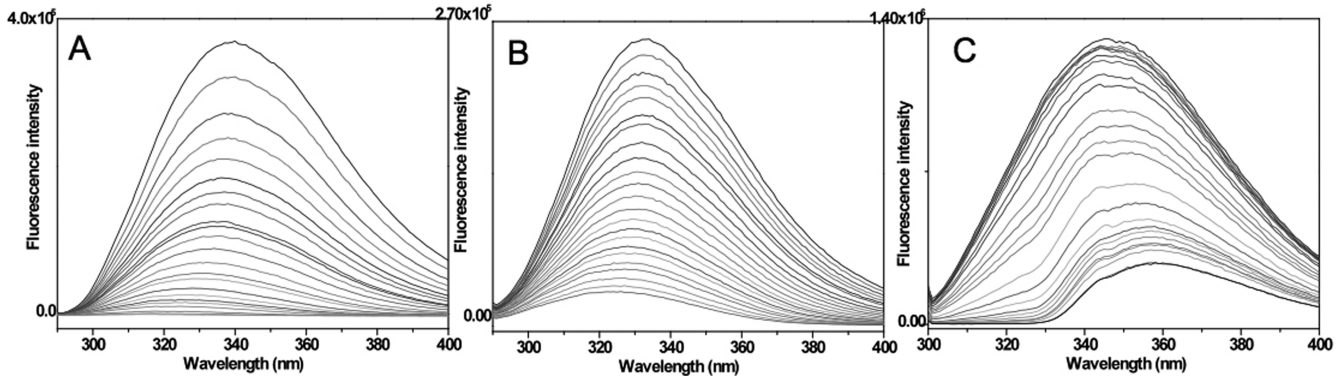

Figure 7. Tryptophan fluorescence quenching behavior of PpIX and PK11195. Tryptophan fluorescence spectra of (A) *Rs*TSPO when binding with PpIX in 0.2% DM, (B) *Hs*TSPO when binding with PpIX in 0.2% DM, and (C) *Rs*TSPO when binding with PK11195 in 0.2% Fos-Choline-12 (PK11195 titration experiments conducted in 0.2% DM show the same spectral behavior as the experiment shown, which was conducted in 0.2% Fos-Choline-12).

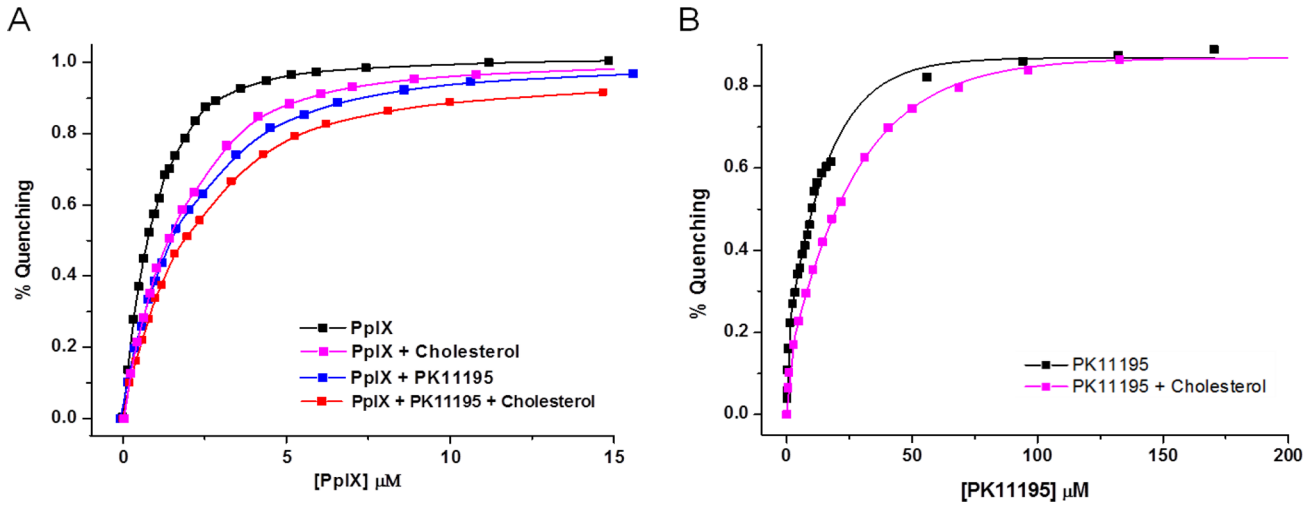

Figure 8. Competition binding studies with PpIX, PK11195, and cholesterol binding to *Rs*TSPO. Experiments were conducted as described in Materials and Methods. (A) Competition between PpIX and cholesterol (preincubated at 50 μM cholesterol) and PK11195 (preincubated at 20 μM PK11195) as well as PK11195 with cholesterol (preincubated with both). (B) Competition between PK11195 and cholesterol (preincubated at 50 μM cholesterol).

shows a broad spectrum from 290 to 400 nm with a peak around 340 nm. PpIX quenches the tryptophan fluorescence evenly at all wavelengths and shows a maximal quenching close to 100% (Figure 7A,B). This indicates that the local environment of almost all tryptophans that contribute to the total tryptophan fluorescence for *Rs*TSPO is influenced by the binding of PpIX. In contrast, PK11195 quenches the fluorescence of *Rs*TSPO from 290 to 335 nm completely but not in the region of 330−340 nm (Figure 7C). This behavior suggests that PK11195 is interacting with a slightly different subset of the tryptophans compared to PpIX, implying some differences in their binding sites in the case of *Rs*TSPO.

To further investigate possible overlap between the binding sites, competition binding assays were performed with PpIX, PK11195, and cholesterol (Figure 8). Purified *Rs*TSPO was preincubated with either 50 μM cholesterol, 20 μM PK11195, or both on ice before the binding experiment.

The binding behavior of PpIX was somewhat affected by the presence of cholesterol, giving an increase in the K_d of 2−3-fold, suggesting some influence of cholesterol on the PpIX binding site. Interestingly, the presence of PK11195 caused a similar change in the binding of PpIX, an ∼3-fold increase in K_d, and PK11195 and cholesterol together had a greater effect (an ∼4-fold increase in K_d). This behavior (Figure 8) suggests that PK11195 and PpIX binding sites are interacting and that cholesterol is also altering the PpIX binding in manner that is somewhat additive with PK11195, consistent with partial overlap or allosteric effects of ligand binding at different sites.

Compounds Affecting Apoptosis Bind to *Rs*TSPO with Micromolar Affinity. Besides the TSPO ligands PK11195, benzodiazepines, and PpIX, which all have been reported to either induce or prevent apoptosis,[27] other compounds have been reported to affect apoptosis in human cell lines, but their targets are not well-defined. In *R. sphaeroides*, TSPO is reported to facilitate the transport of intermediates of heme and carotenoid biosynthesis−breakdown pathways through the outer membrane.[31,33,34] Interestingly, in mammals, the porphyrin breakdown product bilirubin and some carotenoid homologues (retinoids) have also been reported to induce apoptosis through the mitochondrial pathway.[65−67] These and other compounds reported to have effects on MPTP and apoptosis, including curcumin[68] and gossypol,[69] were selected to test for their binding affinity for *Rs*TSPO. Binding studies with both the wild type and the W38C mutant show that

dx.doi.org/10.1021/bi400431t | *Biochemistry* 2013, 52, 5884−5899

several of these compounds bind to purified *Rs*TSPO at low micromolar affinity similar to that of PpIX (Figure 9 and Table 2), which is suggestive that some of these apoptosis-inducing agents could function through direct interaction with TSPO.

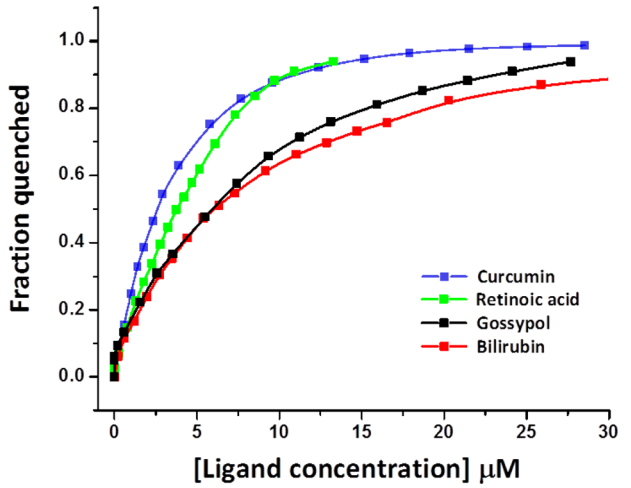

Figure 9. Binding curves of compounds affecting apoptosis: curcumin, retinoic acid, gossypol, and bilirubin.

Models of the *Rs*TSPO Dimer. The structural model of the *Rs*TSPO dimer was constructed using EM-Fold and Rosetta guided by the 10 Å cryo-EM density map of *Rs*TSPO.[46] The two top-scoring models are displayed in Figure 10. The next five top-scoring topologies are provided in Figure S3 of the Supporting Information for comparison. At 10 Å resolution in the cryo-EM experiment, the connectivity between transmembrane helices was not resolved. The objective of the modeling study was to complete the model and use the Rosetta energy function to identify the global energy minimum, thereby adding atomic detail not visible in the experimental data. The seven topologies shown are energetically significantly more favorable than all alternative topologies (Figure S4 of the Supporting Information). The two top-scoring topologies have a significant energy gap of 28 to the top-scoring model of an alternative topology. Therefore, we consider these two topologies as being most likely for *Rs*TSPO.

Some common features are observed in the two top-scoring models, although the two *Rs*TSPO monomers are placed in opposite orientations within the EM density and have a different dimer interface (Figure 10). Both models place helix I and helix V close to each other, consistent with previous mutagenesis data.[35] In addition, helix I and helix II are on the same face, providing the possibility of helices I and II playing a role in substrate binding and transport together (see Discussion for details). The main differences are as follows. (1) Model 1 placed helix V in the dimer interface, while the dimer interface in model 2 is composed of helices I–III. (2) Model 1 has a relatively shorter loop 1, and a portion of predicted loop 1 forms a short helix that contributes to part of the transmembrane region, as compared to that in model 2. However, ligand binding at loop 1 is very likely to change the structure of this flexible region. Considering that TSPO has been reported to form higher-order oligomers,[61] we fit the dimer into the larger density of the *Rs*TSPO helical crystal (Figure S5 of the Supporting Information) and found an additional (though less strong) dimer interface mediated by helices I and II in model 1, as well as an additional dimer interface mediated by helices I and V in model 2. We have focused our binding analysis on model 2, which portrays helices I and II as being at the dimer interface while helix V is at the outside, leaving open the possibility of helix V interacting with another monomer, as suggested in Figure S3 of the Supporting Information, or a partner protein for cholesterol translocation, as suggested by Papadopoulos et al.[57]

DISCUSSION

The ability of TSPO to bind to various ligands has been extensively investigated over the past 30 years, providing important information that has led to our current understanding of the function of TSPO. However, previous studies show significant variation in the binding properties of TSPO when measured in different cell lines, tissues, or purified forms. It has also been suggested that TSPO functions *in vivo* as an oligomer,[61] but details of the oligomerization and conditions that foster it are difficult to establish. To address these and other issues, we purified the homologue of human TSPO from *R. sphaeroides* and characterized the oligomeric state and binding behavior in a well-defined system. The bacterial protein *Rs*TSPO is important in itself, given its role in photosynthetic gene regulation and membrane transport in bacteria. The conserved aspects of sequence, along with some differences in ligand binding between the mammalian and *R. sphaeroides* proteins, provide opportunities to identify the potential determinants for the ligand interactions. In this study, we confirm that *Rs*TSPO forms a dimer *in vitro* and present models with atomic detail for the dimer form. Using one of these models, options for PpIX, PK11195, and cholesterol interaction sites are proposed. The binding behavior of other physiologically important ligands provides some new hints about the mechanism of potential regulation of MPTP by TSPO.

Evidence Relating to the Role of the Dimer. In this work, we characterized the minimal structural unit of purified *Rs*TSPO as a dimer. It is reasonable to postulate that the minimal functional unit of *Rs*TSPO is also a dimer, considering several lines of evidence.

Because TSPO was first discovered and is best known as a receptor, the drug binding properties and the physiological effects of drug-related ligands were initially extensively investigated. However, evidence has been obtained in both mammalian and *Rhodobacter* systems that TSPO also transports molecules, including both cholesterol and the metabolites of heme and photosynthesis pathways.[6,34,62] It is reasonable to propose a monomer form of TSPO functions as a receptor, but given the small size of the protein, it is more difficult to postulate a mechanism for a monomer to transport either cholesterol or the heme/carotenoid metabolic intermediates. Yeliseev and Kaplan proposed that *Rs*TSPO forms a dimer *in vivo*, and this dimer was stabilized by the W38C mutation.[34] Porphyrin has been reported to induce dimerization,[34] although in our hands the already dimeric state of *Rs*TSPO was not influenced by the addition of PpIX. In our studies, no monomer form was ever observed under nondenaturing conditions during chromatography with or without βME, while a trace of dimer remained even under the strong denaturing conditions of urea/SDS–PAGE. In addition, the W38C mutant behaved very much like the wild type in terms of the dimer state, suggesting that *Rs*TSPO naturally forms a dimer by strong associations other than disulfide bonding. Similarly, the *E. coli* drug transporter EmrE[70] forms a dimer in the purified state that is not influenced by ligand binding. Biochemical and NMR data

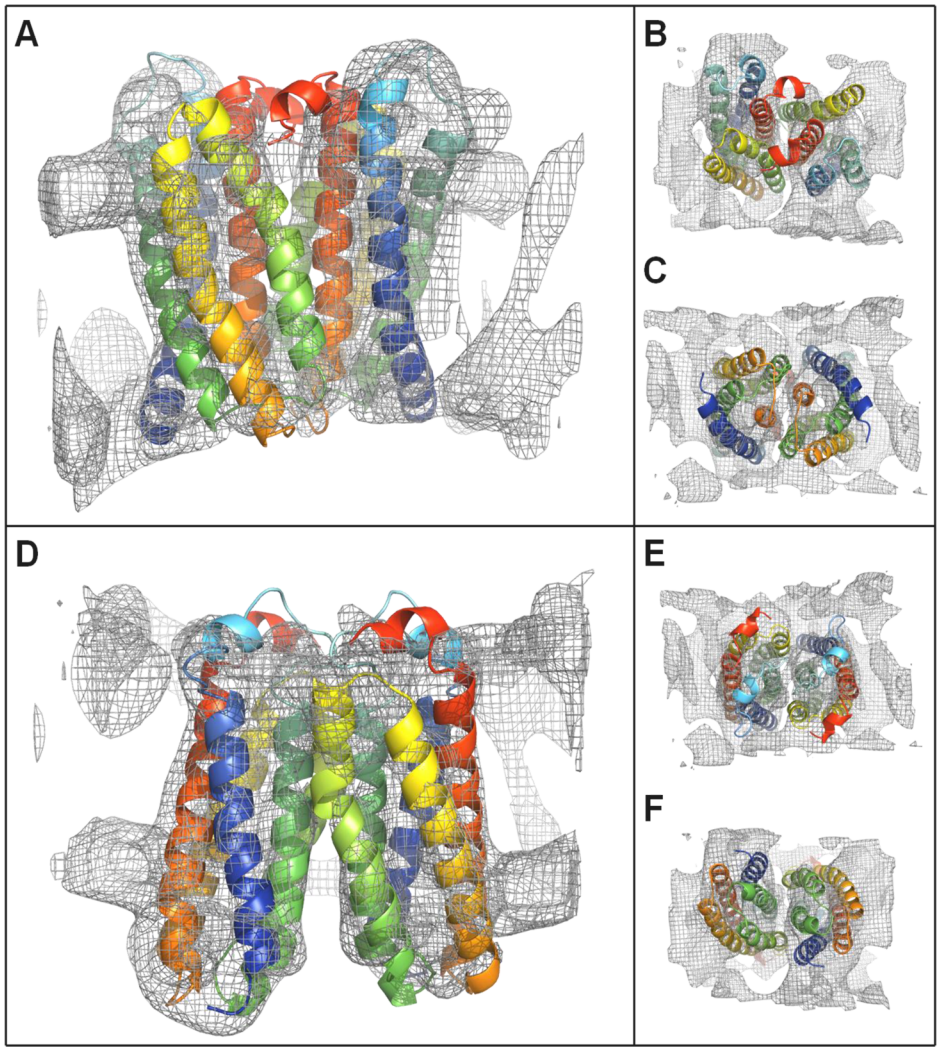

Figure 10. Top two models of a *Rs*TSPO dimer. (A) Side view, (B) top view, and (C) bottom view of model 1. (D) Side view, (E) top view, and (F) bottom view of model 2. Electron density from the EM structure was contoured at 1.5σ. Each monomer is colored with rainbow colors from blue (N-terminus) to red (C-terminus).

also show that EmrE can transport the substrate as a dimer *in vivo*[71] and *in vitro*,[72] while structural studies show a ligand at the dimer interface. In fact, a significant number of transporters function as dimers and/or show 2-fold symmetry with substrate binding at the dimer or domain interface in the crystal structures,[73,74] suggesting a common mechanism for substrate transport that could also apply to TSPO.

In view of the case of EmrE, which shows that a membrane protein can be inserted with dual topology,[56] and given the apparently successful expression of our forced antiparallel dimers, we considered the possibility that TSPO might also function as an antiparallel structure to create a "5 + 5 inverted repeat" topology as reported in several cases.[73,75] Studies (reviewed by Bowie[76]) suggest that rearrangement of the orientation of helices is possible as well as necessary in several cases for both large and small membrane proteins. However, the best cryo-EM and modeling evidence available so far indicates a parallel dimer, as modeled in this paper.

Taken together, our data as well as other studies indicate that *Rs*TSPO functions as a dimer, which is likely to be important for transporting substrates across the membrane. On the other hand, current models regarding the effect of drugs generally agree with the 1:1 drug:monomer ratio, suggesting that TSPO could perform receptor and transporter functions in different oligomer and hetero-oligomer states.

Effect of Detergent on the Structure and Binding of *Rs*TSPO. Detergents play a critical role in the study of membrane proteins, allowing their characterization in a purified state. However, these artificial lipid-mimicking molecules may influence the binding of hydrophobic ligands, as observed in the case of a steroid binding site in cytochrome *c* oxidase where a systematic analysis of detergent effects led to a clearer understanding of competitive behavior between ligands and detergents and a more precise definition of the binding domain.[77,78]

In this study, we also observed the influence of detergent upon the binding of ligands to purified *Rs*TSPO (Figure 5), while Lacapere et al.[27] had previously reported that recombinant mouse TSPO lost its binding to PK11195 when purified with SDS as the detergent but regained its binding ability when reconstituted into liposomes. In their hands, the binding of cholesterol was less influenced than the binding of PK11195 by SDS. In our studies, when a nonionic detergent DM is used, a higher-affinity PK11195 binding site appears to be maintained, as compared to the outcome using the charged detergents Fos-Choline-12 and SDS. Our observations are

dx.doi.org/10.1021/bi400431t | *Biochemistry* 2013, 52, 5884−5899

consistent with the model in which the PK11195 binding site involves flexible extramembrane loop 1 and the membrane interface where detergent/lipid headgroups may have an impact, while cholesterol bound at the more deeply buried CRAC site on helix V may be less impacted by the detergent.

Using the TSPO Dimer Model To Predict the Binding Sites for PpIX, Cholesterol, and PK11195. Although we have demonstrated binding of both PK11195 and cholesterol to purified *Rs*TSPO, it is still a question of what structural features result in an affinity for both ligands that is several orders of magnitudes lower than that in mammalian TSPO. To attempt to obtain new insight into possible ligand interactions, we generated models of *Rs*TSPO in the dimer form (Figure 10). The top-ranked candidate structures were compared, and one (model 2) was used to facilitate an interpretation of the binding of PpIX, cholesterol, and PK11195 to *Rs*TSPO.

Our preliminary competition binding studies (Figure 8) give evidence of some level of interaction among all three binding sites. The effects of PK11195 and cholesterol on the affinity of *Rs*TSPO for PpIX are almost additive, while the binding of PK11195 itself is less influenced by cholesterol. These results are consistent with PK11195 and PpIX interacting at somewhat different positions on extramembrane loop 1, and cholesterol acting at helix V of the C-terminus, with some allosteric influence on both.

We propose that PpIX, as one of the potential endogenous transport substrates of TSPO, binds initially at loop 1, en route to transport via the dimer interface, as illustrated in Figure 11. Previous *in vivo* studies, in particular mutation of residues W30, K36, W38, and W39 in *Rs*TSPO,[34] as well as our data show that loop 1 plays a critical role in the binding and export of porphyrins. However, loop 1 is not likely to be the only contributor to the binding of PpIX. The observation that the tryptophan fluorescence was completely quenched by PpIX but not by PK11195 and other ligands binding (Figure 7) suggests that PpIX either interacts with a rather large area or induces a global conformational change, each of which is possible if PpIX is binding and being transported through the dimer interface. Initial PpIX binding at loop 1 is consistent with our observation that the W38C mutant reduced the affinity of PpIX for *Rs*TSPO by ~6-fold, while aromatic residues on transmembrane helix II, including highly conserved W44 and W50, also appear to play an important role in PpIX binding and transport, as evidenced by the lower porphyrin export activity in phenylalanine mutants of both residues.[34] Our model (Figure 11) is consistent with helix II being a major part of the dimer interface where W44 and W50 are in the region of potentially close interaction with PpIX.

Although PK11195 was also proposed to bind to TSPO at loop 1 and has been reported to compete with PpIX binding,[40] the tryptophan quenching behavior suggests that PK11195 and PpIX do not bind in precisely the same location (Figure 7). As mentioned above, the last two-thirds of the loop 1 is highly conserved across all species, with conserved residues that play critical roles for PpIX binding, while the sequence in the first one-third is not. Thus, the much lower binding affinity of PK11195 for *Rs*TSPO compared to that for *Hs*TSPO could be due in part to differences in the early part of loop 1. However, some overlap between PK11195 and PpIX binding is suggested by competition studies and the fact that the K_d values of both PK11195 and PpIX were markedly reduced by the W38C mutant. On the basis of these independent lines of evidence, here we propose that PK11195 interacts mainly on the first half

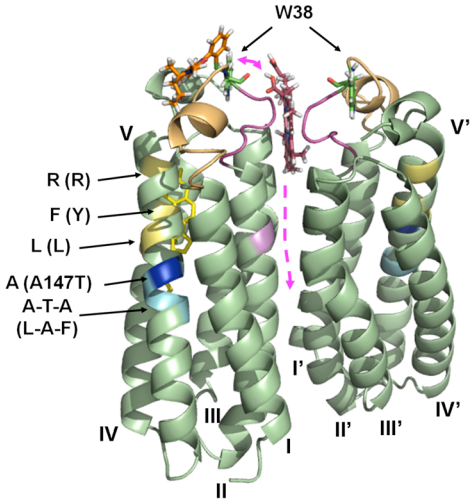

Figure 11. Proposed model of binding sites of PpIX, PK11195, and cholesterol on *Rs*TSPO. Structures of PK11195 and PpIX were generated with ChemDraw 3D, and that of cholesterol was taken from a published structure (PDB entry 3D4S). Note that the computational model of *Rs*TSPO (model 2) is generated on the basis of EM density observed in a sample without ligand. Therefore, these models may represent a closed conformation, as indicated by close association of the monomers. Ligands are manually placed into the model of *Rs*TSPO on one monomer, for the sake of illustration of proposed locations. Helices are labeled with Roman numerals: W38 (green sticks), PK11195 (orange sticks), PpIX (dark purple sticks), and cholesterol (yellow sticks). Highly conserved residues in the CRAC site are colored light yellow and labeled according to the *Rhodobacter* sequence. Corresponding residues in the human sequence are shown in parentheses. Human polymorphism residue A139 (*Rs* number) is colored dark blue, while the preceding Ala-Thr-Ala sequence is colored cyan. The sequence in loop 1, before W38, that is proposed to play a role in PK11195 binding is colored light orange and corresponds to the ligand. The proposed PpIX binding sequence on loop 1 (including W44) is colored light purple, and residue W50 on helix II is colored pink. A loading and transport route for PpIX is indicated by a magenta dotted line, illustrating the potential role of the dimer in transport, which would require flexibility of the external loops.

of loop 1 within the monomer, extending to residue W38 (S41 in human), and also harnesses some of the structural features of the helix I−membrane interface and the second half of loop 1 that binds the hydrophobic porphyrins. This interpretation is consistent with the observation that *Rs*TSPO binds both PK11195 and PpIX with micromolar affinity (Figure 5), while *Hs*TSPO has nanomolar affinity for PK11195 but has an affinity for PpIX similar to that of *Rs*TSPO (Figure 4).[40] Nevertheless, given the flexible nature of the loop, a high-resolution structure with ligand bound will be essential to understanding the details of the binding mechanisms.

In this study, we show that cholesterol does bind to purified *Rs*TSPO but only with low affinity in the high micromolar range. We note that helix V and the C-terminus, where the CRAC sequence is located, are perhaps the most conserved regions in the whole protein. However, the region right before the CRAC is much less conserved and shows some interesting features (Figures 1 and 11). In the human and mouse TSPO proteins, for which nanomolar affinities have been reported, a relatively hydrophobic Leu-Ala-Phe sequence (residues 144−146) precedes the CRAC, whereas in the *R. sphaeroides* sequence, these residues are replaced by an Ala-Thr-Ala sequence (residues 136−138), a much more hydrophilic

combination. In fact, the spontaneous human A147T polymorphism, located right after the Leu-Ala-Phe sequence, has been reported to reduce the level of pregnenolone production[63] and binding of an imaging ligand by 2 orders of magnitude.[38] Our model of *Rs*TSPO (Figure 11) would allow the long hydrophobic tail of cholesterol to extend to the location of the Ala-Thr-Ala sequence, while the ring structure is interacting mainly with the CRAC site. The more hydrophobic character of the human helix V sequence may create a deeper binding site or reposition helix V to favor binding interactions for the hydrophobic rings.

Another interesting question is whether this region of helix V and cholesterol binding also affects other ligands. Besides our observations, extensive investigation of the binding of the original benzodiazepine ligand Ro5-4864 has led to the conclusion that the C-terminal region of TSPO, in particular residues 144−156 of helix V, which include both the CRAC site and the sequence preceding, plays a role in its binding,[35] although the involvement of loop 1 is also observed. The new PET ligand PBR28, a PK11195-related compound, shows a markedly reduced affinity for the *Hs*TSPO polymorphism, A147T.[38] The same mutation in bacterial TSPO was recently reported to disrupt the binding of PpIX.[79] Altogether, helix V and the cholesterol binding region do appear to influence both PpIX and drug ligands. Our two top models (Figure 10 and Figure S3 of the Supporting Information) show that helix V and helix I are in the proximity of each other within the dimer as well as the higher-order oligomer, providing the possibility of direct interaction between binding sites.

From these considerations, a tentative model (Figure 11) for the ligand binding sites of TSPO is proposed, suggesting that TSPO may perform its dual functions as a transporter and a receptor by binding the substrate PpIX at the dimer interface for transporting, while binding PK11195 and other ligands more superficially on loop 1. Cholesterol is proposed to bind at the CRAC site located on helix V, and we cite evidence that the four residues immediately preceding the CRAC site are also important for the binding of cholesterol and other ligands. In model 1, these residues and the cholesterol binding site are located at the dimer interface, suggesting testable differences between the two models.

TSPO as a Mediator of the Regulation of MPTP and Apoptosis. Although numerous studies have implicated TSPO as a regulator of MPTP and apoptosis, the mechanism of the regulation is still unclear. In fact, Gonzalez-Polo et al.[42] reported that the diagnostic TSPO ligand PK11195 shows apoptosis-inducing effects that are independent of TSPO. Another important regulator of MPTP and apoptosis is the B-cell lymphoma 2 (Bcl-2) family of proteins (see the review by Youle and Strasser[80]), which can be either anti-apoptotic, such as Bcl-2 and Bcl-XL, or pro-apoptotic, as in the case of Bax, Bak, and Bid. Bcl-2 family proteins are expressed in the cytosol and recruited during the process of apoptosis to the MPTP on the outer mitochondrial membrane, where TSPO is also localized. The fact that both TSPO and Bcl-2 family proteins regulate apoptosis and the fact that the TSPO ligand PK11195 can reverse the cytoprotective effect of Bcl-2[27] suggest a possible interaction of TSPO and Bcl-2 in the regulation of MPTP.

In this study, we report binding of a number of apoptosis-inducing compounds to purified *Rs*TSPO with low micromolar affinity, including PK11195, retinoic acid, curcumin, and bilirubin. This is consistent with a direct interaction of TSPO with these ligands and supports a role for TSPO during apoptosis. In addition, the binding of a known Bcl-2 inhibitor, gossypol, to purified *Rs*TSPO at low micromolar affinity suggests a relationship between TSPO and Bcl-2 family proteins.

CONCLUSIONS

This study characterizes the oligomeric state of purified TSPO from *R. sphaeroides* as a dimer and reports the binding properties of a variety of ligands. New atomic-resolution models of its dimer form are presented and used to predict TSPO's interaction with various ligands. Several novel ligands are reported, with implications for the role of TSPO in apoptosis and for facilitation of the crystallization of TSPO.

ASSOCIATED CONTENT

Supporting Information

Primer sequences used in this paper (Table T1), the SDS gel of purified *Hs*TSPO (Figure S1), the construction and expression of the dimer fusion proteins (Figure S2), the top 3−7 scoring models of *Rs*TSPO (Figure S3), the comparison of the Rosetta energy functions of the top 20 models generated in this study (Figure S4), and the additional dimer interface of the top two models in the larger oligomer crystal (Figure S5). This material is available free of charge via the Internet at http://pubs.acs.org.

AUTHOR INFORMATION

Corresponding Author

*E-mail: fergus20@msu.edu. Phone: (517) 355-0199.

Funding

This work was supported by Michigan State University Foundation Strategic Partnership Grant "Mitochondrial Science & Medicine" (S.F.-M.), National Institutes of Health Grant GM26916 (S.F.-M.), National Science Foundation Career Award 0742762 (J.M.) and National Institutes of Health Grant R01 GM080403 (J.M.).

Notes

The authors declare no competing financial interest.

The coordinates of the top models reported in this paper are available upon request from J.M. (jens.meiler@vanderbilt.edu).

ACKNOWLEDGMENTS

We thank Dr. Robert Stroud and Dr. Rebecca Robbins at the University of California San Francisco Membrane Protein Expression Center (National Institutes of Health Grant GM 094625 to rms) for support on purification and on the light scattering experiment; Dr. Robert Larkin and Dr. David Kramer for use of the PTI instrument; Dr. Denis Proshlyakov for discussions about data analysis; Qinghui Yuan for generating the *Rs*TSPOW38C mutant during lab rotation; Dr. Vladimir Korkhov and Dr. Christopher Tate for sharing the cryo-electron microscopy density map and the initial coordinates for the helices; and Dr. Carrie Hiser, Dr. Jian Liu, and Lance Valls for technical support. We also thank Dr. Samuel Kaplan for constructs of *Rs*TSPO and Dr. John Lee (University of Minnesota) for initial collaboration on *Rs*TSPO expression.

ABBREVIATIONS

TSPO, Translocator Protein 18 kDa; PBR, peripheral-type benzodiazepine receptor; MPTP, mitochondrial permeability transition pore; VDAC, voltage-dependent anion channel; ANT, adenine nucleotide translocator; *Rs*TSPO, TSPO from

R. sphaeroides; *Hs*TSPO, TSPO from human; CRAC, cholesterol recognition/interaction amino acid consensus; DDM, dodecyl maltoside (lauryl maltoside); DM, decyl maltoside; SDS, sodium dodecyl sulfate; PpIX, protoporphyrin IX; Fos-Choline-12, *n*-dodecylphosphocholine; WT, wild-type; Bcl-2, B-cell lymphoma 2; βME, β-mercaptoethanol; PDB, Protein Data Bank.

REFERENCES

(1) Braestrup, C., and Squires, R. F. (1977) Specific benzodiazepine receptors in rat brain characterized by high-affinity (3H)diazepam binding. *Proc. Natl. Acad. Sci. U.S.A. 74*, 3805−3809.

(2) Papadopoulos, V., Baraldi, M., Guilarte, T. R., Knudsen, T. B., Lacapere, J. J., Lindemann, P., Norenberg, M. D., Nutt, D., Weizman, A., Zhang, M. R., and Gavish, M. (2006) Translocator protein (18 kDa): New nomenclature for the peripheral-type benzodiazepine receptor based on its structure and molecular function. *Trends Pharmacol. Sci. 27*, 402−409.

(3) Fan, J., Lindemann, P., Feuilloley, M. G., and Papadopoulos, V. (2012) Structural and functional evolution of the translocator protein (18 kDa). *Curr. Mol. Med. 12*, 369−386.

(4) Krueger, K. E. (1995) Molecular and functional properties of mitochondrial benzodiazepine receptors. *Biochim. Biophys. Acta 1241*, 453−470.

(5) Anholt, R. R., Pedersen, P. L., De Souza, E. B., and Snyder, S. H. (1986) The peripheral-type benzodiazepine receptor. Localization to the mitochondrial outer membrane. *J. Biol. Chem. 261*, 576−583.

(6) Papadopoulos, V., Amri, H., Boujrad, N., Cascio, C., Culty, M., Garnier, M., Hardwick, M., Li, H., Vidic, B., Brown, A. S., Reversa, J. L., Bernassau, J. M., and Drieu, K. (1997) Peripheral benzodiazepine receptor in cholesterol transport and steroidogenesis. *Steroids 62*, 21−28.

(7) Li, H., and Papadopoulos, V. (1998) Peripheral-type benzodiazepine receptor function in cholesterol transport. Identification of a putative cholesterol recognition/interaction amino acid sequence and consensus patterns. *Endocrinology 139*, 4991−4997.

(8) Taketani, S., Kohno, H., Furukawa, T., and Tokunaga, R. (1995) Involvement of peripheral-type benzodiazepine receptors in the intracellular transport of heme and porphyrins. *J. Biochem. 117*, 875−880.

(9) Verma, A., Nye, J. S., and Snyder, S. H. (1987) Porphyrins Are Endogenous Ligands for the Mitochondrial (Peripheral-Type) Benzodiazepine Receptor. *Proc. Natl. Acad. Sci. U.S.A. 84*, 2256−2260.

(10) Krueger, K. E., and Papadopoulos, V. (1992) Mitochondrial benzodiazepine receptors and the regulation of steroid biosynthesis. *Annu. Rev. Pharmacol. Toxicol. 32*, 211−237.

(11) Chen, M. K., and Guilarte, T. R. (2008) Translocator protein 18 kDa (TSPO): Molecular sensor of brain injury and repair. *Pharmacol. Ther. 118*, 1−17.

(12) Brown, R. C., Degenhardt, B., Kotoula, M., and Papadopoulous, V. (2000) Location-dependent role of the human glioma cell peripheral-type benzodiazepine receptor in proliferation and steroid biosynthesis. *Cancer Lett. 156*, 125−132.

(13) Hardwick, M., Fertikh, D., Culty, M., Li, H., Vidic, B., and Papadopoulos, V. (1999) Peripheral-type benzodiazepine receptor (PBR) in human breast cancer: Correlation of breast cancer cell aggressive phenotype with PBR expression, nuclear localization, and PBR-mediated cell proliferation and nuclear transport of cholesterol. *Cancer Res. 59*, 831−842.

(14) Ji, B., Maeda, J., Sawada, M., Ono, M., Okauchi, T., Inaji, M., Zhang, M. R., Suzuki, K., Ando, K., Staufenbiel, M., Trojanowski, J. Q., Lee, V. M., Higuchi, M., and Suhara, T. (2008) Imaging of peripheral benzodiazepine receptor expression as biomarkers of detrimental versus beneficial glial responses in mouse models of Alzheimer's and other CNS pathologies. *J. Neurosci. 28*, 12255−12267.

(15) Crompton, M. (1999) The mitochondrial permeability transition pore and its role in cell death. *Biochem. J. 341* (Part 2), 233−249.

(16) Decaudin, D., Castedo, M., Nemati, F., Beurdeley-Thomas, A., De Pinieux, G., Caron, A., Pouillart, P., Wijdenes, J., Rouillard, D., Kroemer, G., and Poupon, M. F. (2002) Peripheral benzodiazepine receptor ligands reverse apoptosis resistance of cancer cells in vitro and in vivo. *Cancer Res. 62*, 1388−1393.

(17) Campanella, M. (2012) Editorial: The physiology and pharmacology of the mitochondrial 18 kDa translocator protein (TSPO): An emerging molecular target for diagnosis and therapy. *Curr. Mol. Med. 12*, 355.

(18) Gatliff, J., and Campanella, M. (2012) The 18 kDa translocator protein (TSPO): A new perspective in mitochondrial biology. *Curr. Mol. Med. 12*, 356−368.

(19) Rupprecht, R., Papadopoulos, V., Rammes, G., Baghai, T. C., Fan, J., Akula, N., Groyer, G., Adams, D., and Schumacher, M. (2010) Translocator protein (18 kDa) (TSPO) as a therapeutic target for neurological and psychiatric disorders. *Nat. Rev. Drug Discovery 9*, 971−988.

(20) Xiao, J., Liang, D., Zhang, H., Liu, Y., Li, F., and Chen, Y. H. (2010) 4′-Chlorodiazepam, a translocator protein (18 kDa) antagonist, improves cardiac functional recovery during postischemia reperfusion in rats. *Exp. Biol. Med. 235*, 478−486.

(21) Kroemer, G., Dallaporta, B., and Resche-Rigon, M. (1998) The mitochondrial death/life regulator in apoptosis and necrosis. *Annu. Rev. Physiol. 60*, 619−642.

(22) Tait, S. W., and Green, D. R. (2010) Mitochondria and cell death: Outer membrane permeabilization and beyond. *Nat. Rev. Mol. Cell Biol. 11*, 621−632.

(23) Jiang, X., and Wang, X. (2004) Cytochrome C-mediated apoptosis. *Annu. Rev. Biochem. 73*, 87−106.

(24) McEnery, M. W., Snowman, A. M., Trifiletti, R. R., and Snyder, S. H. (1992) Isolation of the mitochondrial benzodiazepine receptor: Association with the voltage-dependent anion channel and the adenine nucleotide carrier. *Proc. Natl. Acad. Sci. U.S.A. 89*, 3170−3174.

(25) Leung, A. W., and Halestrap, A. P. (2008) Recent progress in elucidating the molecular mechanism of the mitochondrial permeability transition pore. *Biochim. Biophys. Acta 1777*, 946−952.

(26) Giorgio, V., von Stockum, S., Antoniel, M., Fabbro, A., Fogolari, F., Forte, M., Glick, G. D., Petronilli, V., Zoratti, M., Szabó, I., Lippe, G., and Bernardi, P. (2013) Dimers of mitochondrial ATP synthase form the permeability transition pore. *Proc. Natl. Acad. Sci. U.S.A. 110*, 5887−5892.

(27) Krestinina, O. V., Grachev, D. E., Odinokova, I. V., Reiser, G., Evtodienko, Y. V., and Azarashvili, T. S. (2009) Effect of peripheral benzodiazepine receptor (PBR/TSPO) ligands on opening of Ca^{2+}-induced pore and phosphorylation of 3.5-kDa polypeptide in rat brain mitochondria. *Biochemistry (Moscow, Russ. Fed.) 74*, 421−429.

(28) Bui, E. T., Bradley, P. J., and Johnson, P. J. (1996) A common evolutionary origin for mitochondria and hydrogenosomes. *Proc. Natl. Acad. Sci. U.S.A. 93*, 9651−9656.

(29) Armstrong, G. A., Alberti, M., Leach, F., and Hearst, J. E. (1989) Nucleotide sequence, organization, and nature of the protein products of the carotenoid biosynthesis gene cluster of *Rhodobacter capsulatus*. *Mol. Gen. Genet. 216*, 254−268.

(30) Baker, M. E., and Fanestil, D. D. (1991) Mammalian peripheral-type benzodiazepine receptor is homologous to CrtK protein of *Rhodobacter capsulatus*, a photosynthetic bacterium. *Cell 65*, 721−722.

(31) Yeliseev, A. A., and Kaplan, S. (1995) A sensory transducer homologous to the mammalian peripheral-type benzodiazepine receptor regulates photosynthetic membrane complex formation in *Rhodobacter sphaeroides* 2.4.1. *J. Biol. Chem. 270*, 21167−21175.

(32) Yeliseev, A. A., Krueger, K. E., and Kaplan, S. (1997) A mammalian mitochondrial drug receptor functions as a bacterial "oxygen" sensor. *Proc. Natl. Acad. Sci. U.S.A. 94*, 5101−5106.

(33) Yeliseev, A. A., and Kaplan, S. (1999) A novel mechanism for the regulation of photosynthesis gene expression by the TspO outer membrane protein of *Rhodobacter sphaeroides* 2.4.1. *J. Biol. Chem. 274*, 21234−21243.

(34) Yeliseev, A. A., and Kaplan, S. (2000) TspO of *Rhodobacter sphaeroides*. A structural and functional model for the mammalian peripheral benzodiazepine receptor. *J. Biol. Chem. 275*, 5657−5667.
(35) Scarf, A. M., Auman, K. M., and Kassiou, M. (2012) Is there any correlation between binding and functional effects at the translocator protein (TSPO) (18 kDa)? *Curr. Mol. Med. 12*, 387−397.
(36) Li, H., Yao, Z., Degenhardt, B., Teper, G., and Papadopoulos, V. (2001) Cholesterol binding at the cholesterol recognition/interaction amino acid consensus (CRAC) of the peripheral-type benzodiazepine receptor and inhibition of steroidogenesis by an HIV TAT-CRAC peptide. *Proc. Natl. Acad. Sci. U.S.A. 98*, 1267−1272.
(37) Rohmer, M., Bouviernave, P., and Ourisson, G. (1984) Distribution of Hapanoid Triperpene in Prokaryotes. *J. Gen. Microbiol. 30*, 1137−1150.
(38) Owen, D. R., Yeo, A. J., Gunn, R. N., Song, K., Wadsworth, G., Lewis, A., Rhodes, C., Pulford, D. J., Bennacef, I., Parker, C. A., StJean, P. L., Cardon, L. R., Mooser, V. E., Matthews, P. M., Rabiner, E. A., and Rubio, J. P. (2012) An 18-kDa translocator protein (TSPO) polymorphism explains differences in binding affinity of the PET radioligand PBR28. *J. Cereb. Blood Flow Metab. 32*, 1−5.
(39) Lacapère, J. J., and Papadopoulos, V. (2003) Peripheral-type benzodiazepine receptor: Structure and function of a cholesterol-binding protein in steroid and bile acid biosynthesis. *Steroids 68*, 569−585.
(40) Wendler, G., Lindemann, P., Lacapère, J. J., and Papadopoulos, V. (2003) Protoporphyrin IX binding and transport by recombinant mouse PBR. *Biochem. Biophys. Res. Commun. 311*, 847−852.
(41) Scarf, A. M., Luus, C., Da Pozzo, E., Selleri, S., Guarino, C., Martini, C., Ittner, L. M., and Kassiou, M. (2012) Evidence for complex binding profiles and species differences at the translocator protein (TSPO) (18 kDa). *Curr. Mol. Med. 12*, 488−493.
(42) Gonzalez-Polo, R. A., Carvalho, G., Braun, T., Decaudin, D., Fabre, C., Larochette, N., Perfettini, J. L., Djavaheri-Mergny, M., Youlyouz-Marfak, I., Codogno, P., Raphael, M., Feuillard, J., and Kroemer, G. (2005) PK11195 potently sensitizes to apoptosis induction independently from the peripheral benzodiazepin receptor. *Oncogene 24*, 7503−7513.
(43) Decaudin, D., Castedo, M., Nemati, F., Beurdeley-Thomas, A., De Pinieux, G., Caron, A., Pouillart, P., Wijdenes, J., Rouillard, D., Kroemer, G., and Poupon, M. F. (2002) Peripheral benzodiazepine receptor ligands reverse apoptosis resistance of cancer cells in vitro and in vivo. *Cancer Res. 62*, 1388−1393.
(44) Obame, F. N., Zini, R., Souktani, R., Berdeaux, A., and Morin, D. (2007) Peripheral benzodiazepine receptor-induced myocardial protection is mediated by inhibition of mitochondrial membrane permeabilization. *J. Pharmacol. Exp. Ther. 323*, 336−345.
(45) Schaller, S., Paradis, S., Ngoh, G. A., Assaly, R., Buisson, B., Drouot, C., Ostuni, M. A., Lacapere, J. J., Bassissi, F., Bordet, T., Berdeaux, A., Jones, S. P., Morin, D., and Pruss, R. M. (2010) TRO40303, a new cardioprotective compound, inhibits mitochondrial permeability transition. *J. Pharmacol. Exp. Ther. 333*, 696−706.
(46) Korkhov, V. M., Sachse, C., Short, J. M., and Tate, C. G. (2010) Three-dimensional structure of TspO by electron cryomicroscopy of helical crystals. *Structure 18*, 677−687.
(47) Woetzel, N., Lindert, S., Stewart, P. L., and Meiler, J. (2011) BCL::EM-Fit: Rigid body fitting of atomic structures into density maps using geometric hashing and real space refinement. *J. Struct. Biol. 175*, 264−276.
(48) Higuchi, R., Krummel, B., and Saiki, R. K. (1988) A general method of in vitro preparation and specific mutagenesis of DNA fragments: Study of protein and DNA interactions. *Nucleic Acids Res. 16*, 7351−7367.
(49) Studier, F. W. (2005) Protein production by auto-induction in high density shaking cultures. *Protein Expression Purif. 41*, 207−234.
(50) Slotboom, D. J., Duurkens, R. H., Olieman, K., and Erkens, G. B. (2008) Static light scattering to characterize membrane proteins in detergent solution. *Methods 46*, 73−82.
(51) Pettersen, E. F., Goddard, T. D., Huang, C. C., Couch, G. S., Greenblatt, D. M., Meng, E. C., and Ferrin, T. E. (2004) UCSF Chimera: A visualization system for exploratory research and analysis. *J. Comput. Chem. 25*, 1605−1612.
(52) Karakaş, M., Woetzel, N., Staritzbichler, R., Alexander, N., Weiner, B. E., and Meiler, J. (2012) BCL::Fold: De novo prediction of complex and large protein topologies by assembly of secondary structure elements. *PLoS One 7*, e49240.
(53) DiMaio, F., Leaver-Fay, A., Bradley, P., Baker, D., and Andre, I. (2011) Modeling symmetric macromolecular structures in Rosetta3. *PLoS One 6*, e20450.
(54) DiMaio, F., Tyka, M. D., Baker, M. L., Chiu, W., and Baker, D. (2009) Refinement of protein structures into low-resolution density maps using Rosetta. *J. Mol. Biol. 392*, 181−190.
(55) Yarov-Yarovoy, V., Schonbrun, J., and Baker, D. (2006) Multipass membrane protein structure prediction using Rosetta. *Proteins 62*, 1010−1025.
(56) Nasie, I., Steiner-Mordoch, S., Gold, A., and Schuldiner, S. (2010) Topologically random insertion of EmrE supports a pathway for evolution of inverted repeats in ion-coupled transporters. *J. Biol. Chem. 285*, 15234−15244.
(57) Rone, M. B., Liu, J., Blonder, J., Ye, X., Veenstra, T. D., Young, J. C., and Papadopoulos, V. (2009) Targeting and insertion of the cholesterol-binding translocator protein into the outer mitochondrial membrane. *Biochemistry 48*, 6909−6920.
(58) Brambillasca, S., Yabal, M., Makarow, M., and Borgese, N. (2006) Unassisted translocation of large polypeptide domains across phospholipid bilayers. *J. Cell Biol. 175*, 767−777.
(59) Otera, H., Taira, Y., Horie, C., Suzuki, Y., Suzuki, H., Setoguchi, K., Kato, H., Oka, T., and Mihara, K. (2007) A novel insertion pathway of mitochondrial outer membrane proteins with multiple transmembrane segments. *J. Cell Biol. 179*, 1355−1363.
(60) Verma, A., Facchina, S. L., Hirsch, D. J., Song, S. Y., Dillahey, L. F., Williams, J. R., and Snyder, S. H. (1998) Photodynamic tumor therapy: Mitochondrial benzodiazepine receptors as a therapeutic target. *Mol. Med. 4*, 40−45.
(61) Delavoie, F., Li, H., Hardwick, M., Robert, J. C., Giatzakis, C., Péranzi, G., Yao, Z. X., Maccario, J., Lacapère, J. J., and Papadopoulos, V. (2003) In vivo and in vitro peripheral-type benzodiazepine receptor polymerization: Functional significance in drug ligand and cholesterol binding. *Biochemistry 42*, 4506−4519.
(62) Li, H., and Papadopoulos, V. (1998) Peripheral-type benzodiazepine receptor function in cholesterol transport. Identification of a putative cholesterol recognition/interaction amino acid sequence and consensus pattern. *Endocrinology 139*, 4991−4997.
(63) Costa, B., Pini, S., Gabelloni, P., Da Pozzo, E., Abelli, M., Lari, L., Preve, M., Lucacchini, A., Cassano, G. B., and Martini, C. (2009) The spontaneous Ala147Thr amino acid substitution within the translocator protein influences pregnenolone production in lymphomonocytes of healthy individuals. *Endocrinology 150*, 5438−5445.
(64) Taketani, S., Kohno, H., Furukawa, T., and Tokunaga, R. (1995) Involvement of Peripheral-Type Benzodiazepine Receptors in the Intracellular-Transport of Heme and Porphyrins. *J. Biochem. 117*, 875−880.
(65) Keshavan, P., Schwemberger, S. J., Smith, D. L., Babcock, G. F., and Zucker, S. D. (2004) Unconjugated bilirubin induces apoptosis in colon cancer cells by triggering mitochondrial depolarization. *Int. J. Cancer 112*, 433−445.
(66) Korichneva, I., Waka, J., and Hammerling, U. (2003) Regulation of the cardiac mitochondrial membrane potential by retinoids. *J. Pharmacol. Exp. Ther. 305*, 426−433.
(67) Pfahl, M., and Piedrafita, F. J. (2003) Retinoid targets for apoptosis induction. *Oncogene 22*, 9058−9062.
(68) Choudhuri, T., Pal, S., Agwarwal, M. L., Das, T., and Sa, G. (2002) Curcumin induces apoptosis in human breast cancer cells through p53-dependent Bax induction. *FEBS Lett. 512*, 334−340.
(69) Oliver, C. L., Miranda, M. B., Shangary, S., Land, S., Wang, S., and Johnson, D. E. (2005) (−)-Gossypol acts directly on the mitochondria to overcome Bcl-2- and Bcl-X(L)-mediated apoptosis resistance. *Mol. Cancer Ther. 4*, 23−31.

(70) Butler, P. J., Ubarretxena-Belandia, I., Warne, T., and Tate, C. G. (2004) The *Escherichia coli* multidrug transporter EmrE is a dimer in the detergent-solubilised state. *J. Mol. Biol. 340*, 797−808.
(71) Lloris-Garcerá, P., Bianchi, F., Slusky, J. S., Seppälä, S., Daley, D. O., and von Heijne, G. (2012) Antiparallel dimers of the small multidrug resistance protein EmrE are more stable than parallel dimers. *J. Biol. Chem. 287*, 26052−26059.
(72) Morrison, E. A., DeKoster, G. T., Dutta, S., Vafabakhsh, R., Clarkson, M. W., Bahl, A., Kern, D., Ha, T., and Henzler-Wildman, K. A. (2012) Antiparallel EmrE exports drugs by exchanging between asymmetric structures. *Nature 481*, 45−50.
(73) Radestock, S., and Forrest, L. R. (2011) The alternating-access mechanism of MFS transporters arises from inverted-topology repeats. *J. Mol. Biol. 407*, 698−715.
(74) Forrest, L. R., Krämer, R., and Ziegler, C. (2011) The structural basis of secondary active transport mechanisms. *Biochim. Biophys. Acta 1807*, 167−188.
(75) Krishnamurthy, H., Piscitelli, C. L., and Gouaux, E. (2009) Unlocking the molecular secrets of sodium-coupled transporters. *Nature 459*, 347−355.
(76) Bowie, J. U. (2013) Structural biology. Membrane protein twists and turns. *Science 339*, 398−399.
(77) Qin, L., Mills, D. A., Buhrow, L., Hiser, C., and Ferguson-Miller, S. (2008) A conserved steroid binding site in cytochrome *c* oxidase. *Biochemistry 47*, 9931−9933.
(78) Hiser, C., Buhrow, L., Liu, J., Kuhn, L. A., and Ferguson-Miller, S. M. (2013) A Conserved Amphipathic Ligand Binding Region Influences K-Path Dependent Activity of Cytochrome *c* Oxidase. *Biochemistry 52*, 1385−1396.
(79) Ginter, C., Kiburu, I., and Boudker, O. (2013) Chemical Catalysis by the Translocator Protein (18 kDa). *Biochemistry 52*, 3609−3611.
(80) Youle, R. J., and Strasser, A. (2008) The BCL-2 protein family: Opposing activities that mediate cell death. *Nat. Rev. Mol. Cell Biol. 9*, 47−59.
(81) Cserzö, M., Wallin, E., Simon, I., von Heijne, G., and Elofsson, A. (1997) Prediction of transmembrane α-helices in prokaryotic membrane proteins: The dense alignment surface method. *Protein Eng. 10*, 673−676.
(82) Bond, C. S., and Schüttelkopf, A. W. (2009) ALINE: A WYSIWYG protein-sequence alignment editor for publication-quality alignments. *Acta Crystallogr. D65*, 510−512.